Materials Advances

ROYAL SOCIETY OF CHEMISTRY

PAPER

View Article Online
View Journal | View Issue

Cite this: *Mater. Adv.*, 2020, 1, 760

A three-dimensional porous MoS_2–PVP aerogel as a highly efficient and recyclable sorbent for oils and organic solvents†

Pin Song, *[a] Jun Di, [a] Haiping Chen,[b] Sirui Zhao,[c] Cao Wu,[d] Xun Cao, [a] Meiling Wang, [e] Jun Xiong*[f] and Xinli Ye[d]

Received 18th April 2020,
Accepted 3rd June 2020

DOI: 10.1039/d0ma00219d

rsc.li/materials-advances

Three-dimensional (3D) aerogels have attracted more and more attention in oil–water separation, due to their advantages of low density, high porosity, and large specific surface area. However, their application is greatly limited due to their hydrophilic and low adsorption properties. In this work, we report a 3D MoS_2–polyvinylpyrrolidone (PVP) aerogel, prepared by a freeze-drying method, where PVP was used as a skeleton to support the aerogel. As a surfactant, PVP can easily attach to the surface of MoS_2 nanosheets and facilitate the interconnection between nanosheets. The 3D MoS_2–PVP aerogel exhibits low density, high porosity, good hydrophobicity, and excellent adsorption capacity (195–649 times). Moreover, after 30 cycles, the structure of the 3D MoS_2–PVP aerogel is well kept and the adsorption capacity is still retained, at 93.5% and 92.9%, by squeezing and distillation, respectively. Therefore, the obtained 3D MoS_2–PVP aerogel is a promising adsorption material and has great practical application potential in oil–water separation.

Introduction

With the development of society, the problem of water pollution will become more and more serious. Oil leakage, industrial wastewater discharge, and organic solvent leakage are the main causes of water pollution. These problems have caused a serious ecological crisis, which has been the focus of wide attention in basic and applied research all over the world.[1–4] Some traditional approaches were adopted to solve this serious problem, for example, including dispersants, adsorbent materials, oil skimmer vessels, and oil containment booms.[5–13] Among the above methods, using an adsorbent material is one of the most promising approaches because of its simple process and excellent adsorption efficiency.

Porous materials have been widely used as absorbents because they can separate oil and water through a simple and effective absorption process.[14–17] Generally, the ideal absorbent material should have low density, high adsorption capacity, excellent recyclability, and environmental friendliness. Thus, a large number of adsorbent materials have been used to treat sewage, including wool fibers,[18] activated carbon,[19] expanded graphite,[20] and BN nanosheets because of their microporosity.[17,21–23] Although these adsorbent materials are effective to a certain extent, practical application is severely limited due to their low adsorption capacity and poor recyclability. Therefore, it is highly desirable to develop adsorption materials with high adsorption capacity and excellent recyclability.

Recently, the preparation of porous polymer aerogels by a freeze-drying method has been investigated.[24–28] This method exhibits great advantages of simplicity and controllability, which has been widely studied and applied in various fields.[29–33] It has been reported that a GO-PVA aerogel was successfully obtained,[34] as PVA can be used as the skeleton to support GO. A boron nitride-modified PVA aerogel was obtained *via* a freeze-drying method, and it possesses low density, high porosity, and outstanding adsorption capacity for various solvents.[35] MoS_2 is a layered transition metal disulfide with a graphene-like structure.[36] Its unique structure advantages gives it great prospects in the fields of catalysis, batteries, and sensors.[37–42] Due to the extensive study of three-dimensional (3D) aerogels, the demand for MoS_2 aerogels is increasing to realize its potential application.

[a] *School of Materials Science & Engineering, Nanyang Technological University, Singapore 639798, Singapore. E-mail: songpin@ntu.edu.sg*
[b] *School of Mechanics, and Optoelectronic, Physics, Anhui, University, of Science, and Technology, Huainan 232001, P. R. China*
[c] *College of Resources and Environment, Anhui Agricultural University, Hefei 230036, P. R. China*
[d] *College of Materials Science and Technology, Nanjing University of Aeronautics and Astronautics, Nanjing 211106, P. R. China*
[e] *Institute of New Carbon Materials, Taiyuan University of Technology, Taiyuan 030024, Shanxi, China*
[f] *Institute for Energy Research, Jiangsu University, Zhenjiang 212013, P. R. China. E-mail: xiongjun@ujs.edu.cn*

† Electronic supplementary information (ESI) available. See DOI: 10.1039/d0ma00219d

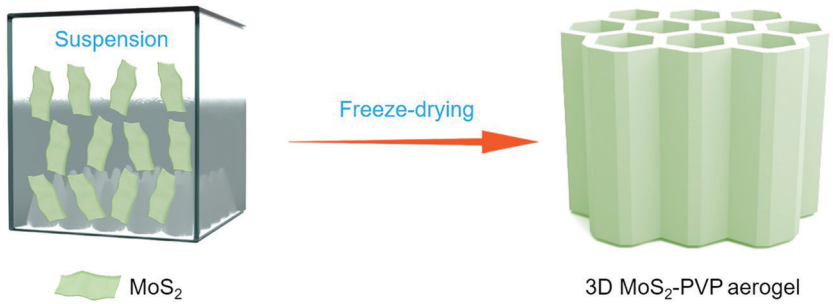

Fig. 1 Assembly process of the 3D MoS_2–PVP aerogel.

Herein, a 3D MoS_2–PVP aerogel has been successfully fabricated using a freeze-drying method. As a surfactant, PVP could easily attach to the surface of MoS_2 nanosheets and facilitate the interconnection between nanosheets. The obtained 3D MoS_2–PVP aerogel exhibits great advantages of high adsorption capacity and strong recyclability. In addition, after 30 cycles, the structure of the 3D MoS_2–PVP aerogel is well kept and the adsorption capacity still retained 93.5% and 92.9%, by squeezing and distillation, respectively. It can be used as a promising adsorption material for environmental remediation.

Results and discussion

Fig. 1 depicts the assembling process of the 3D MoS_2–PVP aerogel. Here, amphiphilic PVP can be used as a framework to support the aerogel (Fig. S1, ESI†). The MoS_2 shows a lateral size of ~200–600 nm (Fig. S2a, ESI†). The specific surface area (SSA) of the pure PVA aerogel is 44.5 $m^2\ g^{-1}$, with the addition of MoS_2, the specific surface area of 3D MoS_2–PVP increased to 75.2, 79.6, 83.5 and 90.4 $m^2\ g^{-1}$, respectively (Table S1, ESI†).

Fig. 2a and b show the XRD patterns of the samples. Two diffraction peaks at 11.3° and 19.7° confirm the amorphous nature of PVP (Fig. 2b). The diffraction peaks of the MoS_2–PVP aerogel match well with those of MoS_2 (Fig. 2a). Nevertheless, it can be seen that the intensity ratio of (002)/(103) of MoS_2–PVP aerogels (7.3) is higher than that of MoS_2 (1.6), confirming that the PVP promotes the exfoliation of the MoS_2 nanosheets.[37,43]

The morphologies of these samples are shown in Fig. S2 (ESI†). Fig. S2a (ESI†) shows that the MoS_2 had a 2D sheet-shaped morphology. In particular, when MoS_2 is combined with PVP, the irregular porous structure of the MoS_2 nanosheets can be obtained (Fig. S2b, ESI†). Furthermore, PVP can easily insert into the MoS_2 nanosheets to generate thinner nanosheets.[43]

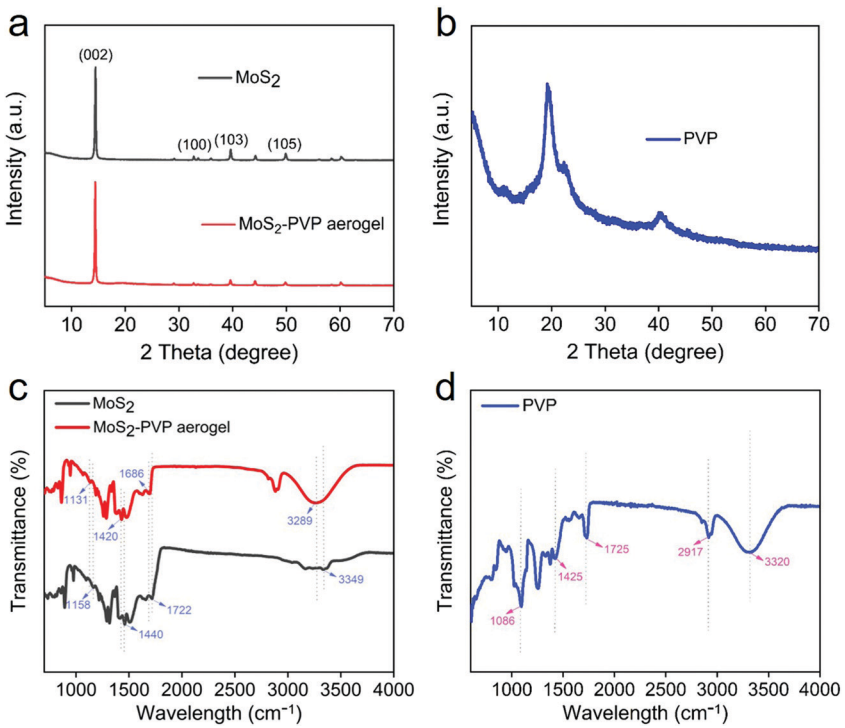

Fig. 2 (a and b) XRD patterns of MoS_2, MoS_2–PVP aerogel and PVP. (c and d) FTIR spectra of MoS_2, MoS_2–PVP aerogel and PVP.

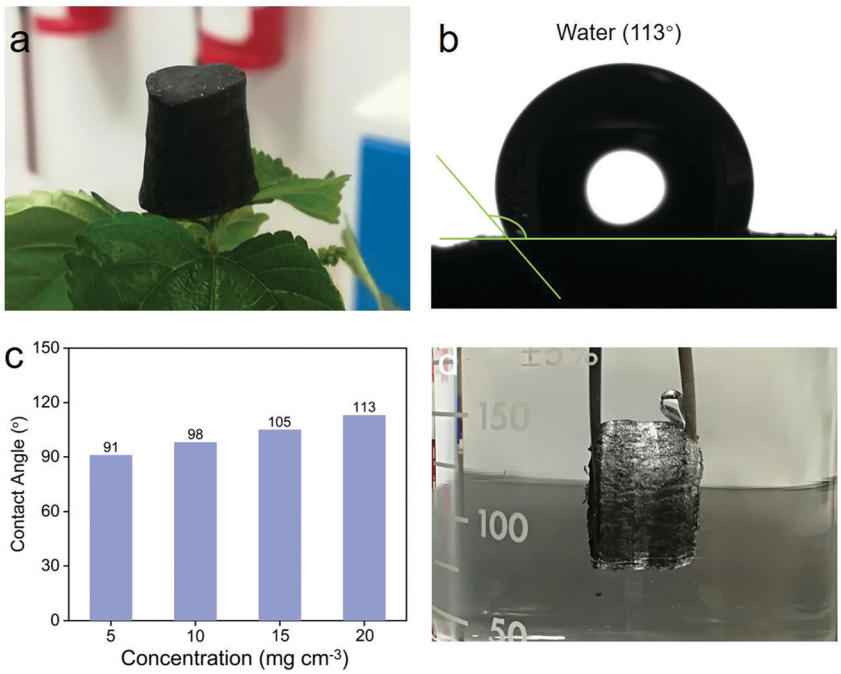

Fig. 3 (a) Photograph of the 3D MoS_2–PVP aerogel standing on a flower surface. (b) Photograph of the WCA of the 3D MoS_2–PVP aerogel. (c) The WCAs of the 3D MoS_2–PVP aerogels with different concentrations of MoS_2. (d) Photograph of mirror-reflection, which further confirms the hydrophobicity of the 3D MoS_2–PVP aerogel.

The FTIR spectra in Fig. 2c and d further indicate the interaction between MoS_2 and PVP. These peaks of PVP at 3320, 2917 and 1425, 1725, 1086 cm^{-1} are attributed to O–H, $-CH_3$, C = O and C–O functional groups, respectively. The peaks of MoS_2 at 3349, 1722, 1440 and 1158 cm^{-1} correspond to O–H, C═O, $-CH_3$ and C–O functional groups, respectively. However, the characteristic peaks of the MoS_2–PVP aerogel blueshift to 3289, 1686, 1420 and 1131 cm^{-1}, indicating the interaction between MoS_2 and PVP.[44]

Fig. S3 (ESI†) contains optical photos of the 3D MoS_2–PVP aerogel with different concentrations of MoS_2, which have basically the same macroscopic morphology. Moreover, the PVP aerogel can also be obtained by the freeze-drying method, which indicates its potential as the 3D framework to support the aerogel. Importantly, our method is widely applicable to the preparation of other 1D or 2D material-PVP aerogels. Taking BN-PVP and CNTs-PVP aerogels as examples, they were also successfully obtained by this method (Fig. S4, ESI†).

It has been reported that a high specific surface area is beneficial for the improvement of adsorption performance.[45] Therefore, we selected the 3D MoS_2–PVP aerogel (20 mg cm^{-3}) with a high specific surface area as the research object. The 3D MoS_2–PVP aerogel can stand stably on the surface of a flower (Fig. 3a). Fig. S5 (ESI†) shows that the 3D MoS_2–PVP aerogel can support water droplets on its surface, ascribed to its good hydrophobicity. The hydrophobicity of the adsorption materials has great significance for the application of oil–water separation. Fig. 3b and c exhibit the water contact angles (WCAs) of the 3D MoS_2–PVP aerogel. The WCAs of the 3D MoS_2–PVP aerogel increase from 91° to 113° with the increase of MoS_2 (Fig. 3c), indicating the hydrophobicity of the 3D MoS_2–PVP aerogel. As shown in Fig. 3d, the mirror-reflection is observed, ascribed to the formation of a new interface between the aerogel and the surrounding water,[46] which further confirms the hydrophobicity of the 3D MoS_2–PVP aerogel.

Furthermore, the 3D MoS_2–PVP aerogel shows excellent mechanical performance. Fig. S6 (ESI†) shows that the compressive curves have good hysteresis loops, which are consistent with the typical behavior of porous materials.[47] With the increase of MoS_2, the mechanical properties improve. When the concentration of MoS_2 is 5 mg cm^{-3}, the compression strength is 4 kPa. The compression strength of MoS_2–PVP was reinforced to 25, 45, and 63 kPa at the concentrations of 10, 15 and 20 mg cm^{-3}, respectively. The result shows that the MoS_2–PVP aerogel had an outstanding compression performance, which may be attributed to the high contribution of the ordered structure.

The 3D MoS_2–PVP aerogel is one of the ideal adsorption materials for removing various oils and organic solvents due to its good hydrophobicity and excellent mechanical stability. As shown in Fig. 4a and Movie S1 (ESI†), when the 3D MoS_2–PVP aerogel is placed on the surface of an oil–water mixture, it can absorb the oil completely and quickly. These results confirm that it has great prospects in the field of oil–water separation.

To explore the adsorption efficiency of the 3D MoS_2–PVP aerogel, the weight gain (wt%) was defined as the adsorbed weight of the solvent per unit weight by the dry aerogel. Herein, Table S1 (ESI†) shows that the SSA of the 3D MoS_2–PVP aerogel is increased with the increasing MoS_2. Moreover, the adsorption capacity of the 3D MoS_2–PVP aerogel increases with the increasing SSA (Fig. S7, ESI†).

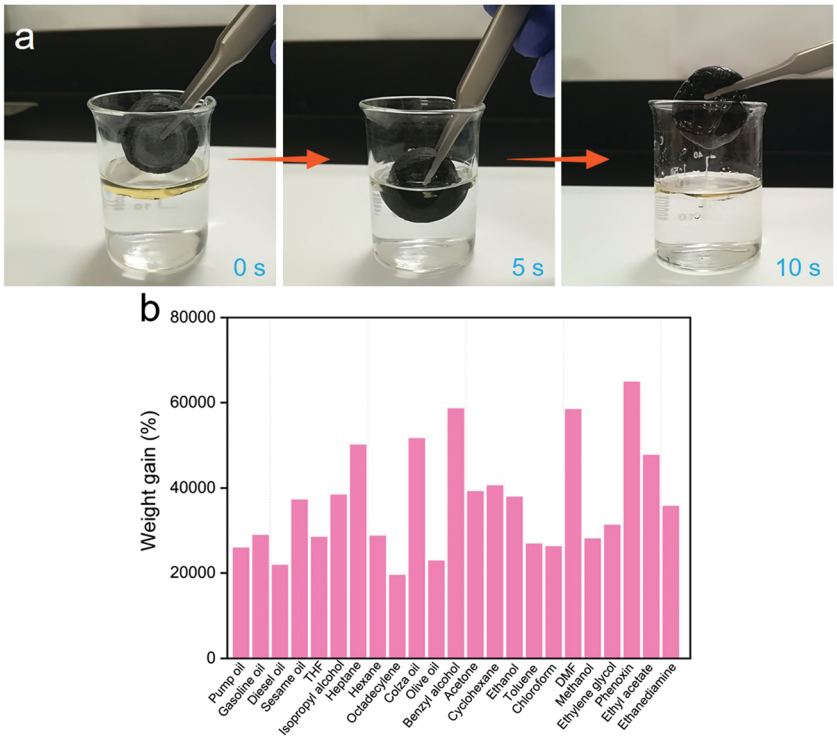

Fig. 4 Absorption performance of the 3D MoS_2–PVP aerogel. (a) Photographs of the absorbed pump oil by the 3D MoS_2–PVP aerogel. (b) The adsorption capacity of the 3D MoS_2–PVP aerogel for various organic solvents and oils.

Table 1 Comparison of various adsorbent materials

Adsorbent materials	Absorbed substances	Sorption capacity (g g^{-1})	Cost	Ref.
Wool-based nonwoven	Diesel, crude oil, SN 150	9–15	Low	48
Graphene/CNT foam	Compressor oil, organic solvents	80–140	High	53
Vegetable fiber	Crude oil	1–100	Low	49
Graphene sponge	Oils and organic solvents	60–160	High	54
Exfoliated graphite	Heavy oil	60–90	Low	51
Carbon nanotube sponge	Oils and organic solvents	80–180	High	50
Magnetic exfoliated graphite	Oils	30–50	High	52
Graphene-based sponge	Oils and organic solvents	60–160	High	46
Reduced graphite oxide foam	Oils and organic solvents	5–40	High	55
SMF foam	Oils and organic solvents	78–172	High	79
CNT sponge-doped graphene foam	Oils and organic solvents	25–125	High	57
BCM sponge	Oils and organic solvents	86–201	High	80
CMB aerogel	Oils and organic solvents	56–188	Low	59
GMF aerogel	Oils and organic solvents	60–140	Low	60
OCA aerogel	Oils and organic solvents	81–171	Low	61
MCF aerogel	Oils and organic solvents	88–228	Low	62
SMS sponge	Oils and organic solvents	82–159	Low	63
MCGA	Oils and organic solvents	80–197	High	64
FGN/PU sponge	Oils and organic solvents	25–44	High	81
HAP nanowire aerogel	Oils and organic solvents	83–156	Low	65
Silylated wood sponge	Oils and organic solvents	16–41	Low	66
Graphene foams	Oils and organic solvents	120–250	High	67
EVOH NFAs	Oils and organic solvents	45–102	Low	68
GCTs	Oils and organic solvents	250–400	High	69
TCF aerogel	Oils and organic solvents	50–192	Low	70
Carbon aerogel	Oils and organic solvents	80–161	High	71
3C aerogels	Oils and organic solvents	33–70	High	72
Co–C/CF sponge	Oils and organic solvents	85–200	High	73
CMA	Oils and organic solvents	78–348	Low	45
3D MoS_2–PVP aerogel	Oils and organic solvents	195–649	Low	This work

SMF: superhydrophobic melamine-formaldehyde, BCM: biomass-decorated carbonaceous melamine, CMB: carbon microbelt, GMF: graphene modified foam, OCA: oleophilic carbon aerogel, MCF: microfibrillated cellulose fibers, SMS: superoleophilic M_OS_2 nanosheet sponge, MCGA: modified cellulose/graphene aerogels, FGN/PU: functionalized graphene/PU, HAP: hydroxyapatite, EVOH NFAs: poly(vinyl alcohol-*co*-ethylene) nanofiber aerogels, GCTs: giant carbon tubes, TCF: twisted carbon fibers, 3C: compressible and conductive carbon, CF: carbon foam, and CMA: carbon microtube aerogel.

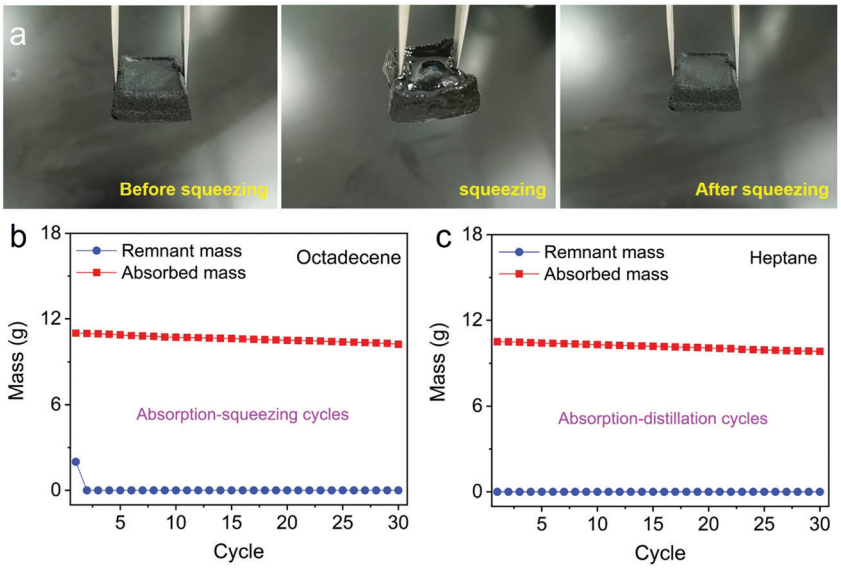

Fig. 5 Recycling of the 3D MoS_2–PVP aerogel. (a) The photographs show the process of adsorption–squeezing. (b) Adsorption-squeezing recycles of the 3D MoS_2–PVP aerogel for the recovery of octadecene. (c) Adsorption–distillation cycles of the 3D MoS_2–PVP aerogel for the recovery of heptane.

The adsorption capability of the 3D MoS_2–PVP aerogel of various oils and organic solvents were measured. The result shows that the 3D MoS_2–PVP aerogel has excellent adsorption capacity and can absorb solvents 195–649 times its own weight (Fig. 4b).

In addition, the adsorption capacity of the 3D MoS_2–PVP aerogel is higher than that of the previously reported adsorption materials (Table 1),[46,48–73] such as exfoliated graphite (60–90 times),[74] carbon nanotube sponge (80–180 times),[50] graphene sponge (60–160 times),[54] and reduced graphite oxide foam (5–40 times).[55] Moreover, the method to prepare the 3D MoS_2–PVP aerogel is relatively simple and its precursor is relatively cheap. Therefore, the obtained 3D MoS_2–PVP aerogel is regarded as the most promising adsorbent for environmental remediation.

The key for oil–water separation is the recyclability of the contaminants, as most contaminants contain both valuable and harmful materials. Two typical methods have been reported for recovering contaminants: squeezing and distillation. As observed in Fig. 5a, the octadecene absorbed by the 3D MoS_2–PVP aerogel can be recovered by squeezing. When the pressure is released, the aerogel can return to its original shape (Fig. 5a).

Moreover, the 3D MoS_2–PVP aerogel was used in recycle tests by squeezing and distillation (Fig. 5b and c). Fig. 5b shows the absorption–squeezing cycle process of the 3D MoS_2–PVP aerogel. The structure of the 3D MoS_2–PVP aerogel was well maintained and the gel still retained an adsorption capacity of 93.5% after 30 cycles (Fig. S8a and b, ESI†). As illustrated in Fig. 5c, the 3D MoS_2–PVP aerogel still retained an adsorption capacity of 92.9% after 30 cycles, which suggests its good recyclability. In addition, the structure of 3D MoS_2–PVP aerogel was well maintained after 30 cycles of the adsorption–distillation process (Fig. S9a and b, ESI†). Therefore, the obtained 3D MoS_2–PVP aerogel can be used to remove contaminants by squeezing, distillation, or a combination of the two methods. It shows a great potential practical application value in the field of oil–water separation.

Conclusions

In conclusion, a 3D MoS_2–PVP aerogel with low density, good hydrophobicity, high adsorption capacity, and excellent recyclability was fabricated by the freeze-drying method. The adsorption capacity of the 3D MoS_2–PVP aerogel can be as high as 195–649 times its own weight. Moreover, after 30 cycles, the structure of the 3D MoS_2–PVP aerogel is well maintained and the gel still retains an adsorption capacity of 93.5% and 92.9% by squeezing and distillation, respectively. Therefore, the obtained 3D MoS_2–PVP aerogel has extremely good potential for applications in oil–water separation.

Experimental section

Materials

MoS_2 powder was purchased from Nanjing XFNANO Materials Tech Co., Ltd. PVP and various organic solvents were from Shanghai Aladdin Biochemistry Technology Co., Ltd. Gasoline oil was provided by the local gas station. Pump oil, sesame oil, colza, and olive oil were obtained in the local market.

Preparation of the 3D MoS_2–PVP aerogel

The 3D MoS_2–PVP aerogel was prepared by the freeze-drying method.[45,75–78] Briefly, MoS_2 powder was uniformly dispersed in PVP solutions (1 mg cm^{-3}) under stirring and the concentration of MoS_2 was set to 5, 10, 15 and 20 mg cm^{-3}, respectively. Then the suspension was poured into a rubber mold placed at the top of a cold steel rod, which was cooled by adding liquid nitrogen

and kept at −70 °C for 1 h. Then the obtained frozen sample was further freeze-dried by using a Labconco-195 freeze-drier for 72 h. Finally, the 3D MoS_2–PVP aerogel was obtained.

Characterization

The morphology was observed by SEM (S-4800, Hitachi) at an accelerating voltage of 10 kV. The X-ray diffraction pattern was obtained using an XRD-6000 (Shimadzu) system with Cu Kα radiation (λ = 1.54178 Å). Fourier transform infrared spectroscopy (FTIR) was characterized from 4000 to 400 cm^{-1} wavenumber by using a Nicolet 6700 instrument. The contact angle with water was characterized by using an OCA 15 Pro instrument. The specific surface area was studied using an ASAP 2020 system at 77 K. The compression tests were carried out using an Instron 5565A system at the speed of 0.1 mm min^{-1}.

Absorption of oils and organic solvents

During the adsorption tests, these 3D MoS_2–PVP aerogels were required to be completely filled with oils or organic solvents. To avoid evaporation of solvents with low boiling points, the weight measurements should be made quickly. The weights of the 3D MoS_2–PVP aerogels before and after adsorption were recorded.

Conflicts of interest

There are no conflicts to declare.

Acknowledgements

This work was supported by the National Natural Science Foundation of China (21606113).

References

1 J. Aurell and B. K. Gullett, *Environ. Sci. Technol.*, 2010, **44**, 9431–9437.
2 K. Jayaramulu, K. K. Datta, C. Rosler, M. Petr, M. Otyepka, R. Zboril and R. A. Fischer, *Angew. Chem., Int. Ed.*, 2016, **55**, 1178–1182.
3 K. Yin, D. Chu, X. Dong, C. Wang, J. A. Duan and J. He, *Nanoscale*, 2017, **9**, 14229–14235.
4 Y. Yang, X. Li, X. Zheng, Z. Chen, Q. Zhou and Y. Chen, *Adv. Mater.*, 2018, **30**, 1704912–1704922.
5 A. Bayat, S. F. Aghamiri, A. Moheb and G. R. Vakili-Nezhaad, *Chem. Eng. Technol.*, 2005, **28**, 1525–1528.
6 M. O. Adebajo, R. L. Frost, J. T. Kloprogge, O. Carmody and S. Kokot, *J. Porous Mater.*, 2003, **10**, 159–170.
7 V. Rajakovic, G. Aleksic, M. Radetic and L. Rajakovic, *J. Hazard. Mater.*, 2007, **143**, 494–499.
8 J. Xiong, P. Song, J. Di, H. M. Li and Z. Liu, *J. Mater. Chem. A*, 2019, **7**, 25203–25226.
9 P. Song, J. Cui, J. Di, D. Liu, M. Xu, B. Tang, Q. Zeng, J. Xiong, C. Wang, Q. He, L. Kang, J. Zhou, R. Duan, B. Chen, S. Guo, F. Liu, J. Shen and Z. Liu, *ACS Nano*, 2020, **14**, 595–602.
10 T. Chen, M. Li, L. Zhou, X. Ding, D. Lin, T. Duan, G. Yang, R. He and W. Zhu, *ACS Sustainable Chem. Eng.*, 2020, **8**, 6458–6465.
11 X. Wang, Z. Han, Y. Liu and Q. Wang, *Appl. Surf. Sci.*, 2020, **505**, 144577–144587.
12 M. Yu, P. Xu, J. Yang, L. Ji and C. Li, *Adv. Mater. Interfaces*, 2020, **7**, 1901671–1901680.
13 J. Gu, H. Fan, C. Li, J. Caro and H. Meng, *Angew. Chem., Int. Ed.*, 2019, **58**, 5297–5301.
14 X. Zhang, Z. Li, K. Liu and L. Jiang, *Adv. Funct. Mater.*, 2013, **23**, 2881–2886.
15 H. Bi, Z. Yin, X. Cao, X. Xie, C. Tan, X. Huang, B. Chen, F. Chen, Q. Yang, X. Bu, X. Lu, L. Sun and H. Zhang, *Adv. Mater.*, 2013, **25**, 5916–5921.
16 X. Gui, Z. Zeng, Z. Lin, Q. Gan, R. Xiang, Y. Zhu, A. Cao and Z. Tang, *ACS Appl. Mater. Interfaces*, 2013, **5**, 5845–5850.
17 W. Lei, D. Portehault, D. Liu, S. Qin and Y. Chen, *Nat. Commun.*, 2013, **4**, 1777–1783.
18 T. R. Annunciado, T. H. Sydenstricker and S. C. Amico, *Mar. Pollut. Bull.*, 2005, **50**, 1340–1346.
19 M. A. Lillo-Ródenas, D. Cazorla-Amorós and A. Linares-Solano, *Carbon*, 2005, **43**, 1758–1767.
20 M. Inagakl, H. Konno, M. Toyoda, K. Moriya and T. Kihara, *Desalination*, 2000, **128**, 213–218.
21 Y. Yu, H. Chen, Y. Liu, V. Craig, L. H. Li and Y. Chen, *Adv. Mater. Interfaces*, 2014, **1**, 1300002–1300006.
22 L. Ci, L. Song, C. Jin, D. Jariwala, D. Wu, Y. Li, A. Srivastava, Z. F. Wang, K. Storr, L. Balicas, F. Liu and P. M. Ajayan, *Nat. Mater.*, 2010, **9**, 430–435.
23 L. Song, L. J. Ci, H. Lu, P. B. Sorokin, C. H. Jin, J. Ni, A. G. Kvashnin, D. G. Kvashnin, J. Lou, B. I. Yakobson and P. M. Ajayan, *Nano Lett.*, 2010, **10**, 3209–3215.
24 H. F. Zhang, I. Hussain, M. Brust, M. F. Butler, S. P. Rannard and A. I. Cooper, *Nat. Mater.*, 2005, **4**, 787–793.
25 R. Y. Zhang, W. C. Wan, L. J. Qiu and Y. Zhou, *Mater. Lett.*, 2016, **181**, 321–324.
26 I. Lee, S.-M. Kang, S.-C. Jang, G.-W. Lee, H. E. Shim, M. Rethinasabapathy, C. Roh and Y. S. Huh, *J. Mater. Chem. A*, 2019, **7**, 1737–1748.
27 Y. A. Haleem, D. B. Liu, W. X. Chen, C. D. Wang, C. H. Hong, Z. He, J. W. Liu, P. Song, S. H. Yu and L. Song, *Composites, Part B*, 2015, **78**, 480–487.
28 M. Xu, R. Yu, Y. Guo, C. Chen, Q. Han, J. Di, P. Song, L. Zheng, Z. Zhang, J. Yan, W. Zhao, J. Yun, C. Liu, Q. Li, Y. Wang, X. Wang and Z. Liu, *Inorg. Chem. Front.*, 2019, **6**, 2801–2809.
29 B. Cao, J. Yin, S. F. Yan, L. Cui, X. S. Chen and Y. T. Xie, *Macromol. Biosci.*, 2011, **11**, 427–434.
30 P. Song, Z. J. Peng, Y. L. Yue, H. Zhang, Z. Zhang and Y. C. Fan, *eXPRESS Polym. Lett.*, 2013, **7**, 546–553.
31 J. Di, C. Chen, C. Zhu, P. Song, J. Xiong, M. X. Ji, J. D. Zhou, Q. D. Fu, M. Z. Xu, W. Hao, J. X. Xia, S. Z. Li, H. M. Li and Z. Liu, *ACS Appl. Mater. Interfaces*, 2019, **11**, 30786–30792.

32 J. Xiong, P. Song, J. Di and H. Li, *Appl. Catal., B*, 2019, **256**, 117788–117802.
33 Y. A. Haleem, P. Song, D. B. Liu, C. D. Wang, W. Gan, M. F. Saleem and L. Song, *Materials*, 2016, **9**, 507–518.
34 J. Dai, T. Huang, S. Q. Tian, Y. J. Xiao, J. H. Yang, N. Zhang, Y. Wang and Z. W. Zhou, *Mater. Des.*, 2016, **107**, 187–197.
35 R. Zhang, W. Wan, L. Qiu, Y. Wang and Y. Zhou, *Appl. Surf. Sci.*, 2017, **419**, 342–347.
36 X. Zhang, X. F. Qiao, W. Shi, J. B. Wu, D. S. Jiang and P. H. Tan, *Chem. Soc. Rev.*, 2015, **44**, 2757–2785.
37 D. Cao, K. Ye, O. A. Moses, W. Xu, D. Liu, P. Song, C. Wu, C. Wang, S. Ding, S. Chen, B. Ge, J. Jiang and L. Song, *ACS Nano*, 2019, **13**, 11733–11740.
38 H. Xu, J. Yi, X. She, Q. Liu, L. Song, S. Chen, Y. Yang, Y. Song, R. Vajtai, J. Lou, H. Li, S. Yuan, J. Wu and P. M. Ajayan, *Appl. Catal., B*, 2018, **220**, 379–385.
39 Q. Liu, X. Li, Q. He, A. Khalil, D. Liu, T. Xiang, X. Wu and L. Song, *Small*, 2015, **11**, 5556–5564.
40 Q. Liu, Q. Fang, W. Chu, Y. Wan, X. Li, W. Xu, M. Habib, S. Tao, Y. Zhou, D. Liu, T. Xiang, A. Khalil, X. Wu, M. Chhowalla, P. M. Ajayan and L. Song, *Chem. Mater.*, 2017, **29**, 4738–4744.
41 W. Zheng, Y. Xu, L. Zheng, C. Yang, N. Pinna, X. Liu and J. Zhang, *Adv. Funct. Mater.*, 2020, **30**, 2000435–2000444.
42 Y. Tian, X. Liu, X. Cao, D. Zhang, S. Xiao, X. Li, Z. Le, X. Li and H. Li, *Chem. Eng. J.*, 2019, **374**, 429–436.
43 J. Liu, Z. Zeng, X. Cao, G. Lu, L. H. Wang, Q. L. Fan, W. Huang and H. Zhang, *Small*, 2012, **8**, 3517–3522.
44 R. Zhang, W. Wan, L. Qiu and Y. Zhou, *Mater. Lett.*, 2016, **181**, 321–324.
45 P. Song, J. W. Cui, J. Di, D. B. Liu, M. Z. Xu, B. J. Tang, Q. S. Zeng, J. Xiong, C. D. Wang, Q. He, L. X. Kang, J. D. Zhou, R. H. Duan, B. B. Chen, S. S. Guo, F. C. Liu, J. Shen and Z. Liu, *ACS Nano*, 2020, **14**, 595–602.
46 D. D. Nguyen, N. H. Tai, S. B. Lee and W. S. Kuo, *Energy Environ. Sci.*, 2012, **5**, 7908–7912.
47 Y. Tang, K. L. Yeo, Y. Chen, L. W. Yap, W. Xiong and W. L. Cheng, *J. Mater. Chem. A*, 2013, **1**, 6723.
48 M. M. Radetić, D. M. Jocić, P. M. Jovančić, Z. L. J. Petrović and H. F. Thomas, *Environ. Sci. Technol.*, 2003, **37**, 1008–1012.
49 T. R. Annunciado, T. H. D. Sydenstricker and S. C. Amico, *Mar. Pollut. Bull.*, 2005, **50**, 1340–1346.
50 X. C. Gui, J. Q. Wei, K. L. Wang, A. Y. Cao, H. W. Zhu, Y. Jia, Q. K. Shu and D. H. Wu, *Adv. Mater.*, 2010, **22**, 617–621.
51 M. Toyoda and M. Inagaki, *Carbon*, 2000, **38**, 199–210.
52 G. L. Wang, Q. R. Sun, Y. Q. Zhang, J. H. Fan and L. M. Ma, *Desalination*, 2010, **263**, 183–188.
53 X. C. Dong, J. Chen, Y. W. Ma, J. Wang, C. P. Mary, B. X. Liu, L. Wang, W. Huang and P. Chen, *Chem. Commun.*, 2012, **48**, 10660.
54 J. P. Zhao, W. C. Ren and H. M. Cheng, *J. Mater. Chem.*, 2012, **22**, 20197–20202.
55 Z. Q. Niu, J. Chen, H. H. Hng, J. Ma and X. D. Chen, *Adv. Mater.*, 2012, **24**, 4144–4150.
56 Y. Zhao, C. G. Hu, Y. Hu, H. H. Cheng, G. Q. Shi and L. T. Qu, *Angew. Chem., Int. Ed.*, 2012, **124**, 11533–11537.
57 D. P. Hashim, N. T. Narayanan, J. M. Romo-Herrera, D. A. Cullen, M. G. Hahm, P. Lezzi, J. R. Suttle, D. Kelkhoff, E. Muñoz-Sandoval and S. Ganguli, *Sci. Rep.*, 2012, **2**, 363.
58 H. Y. Sun, Z. Xu and C. Gao, *Adv. Mater.*, 2013, **25**, 2554–2560.
59 H. C. Bi, X. Huang, X. Wu, X. H. Cao, C. L. Tan, Z. Y. Yin, X. H. Lu, L. T. Sun and H. Zhang, *Small*, 2014, **10**, 3544–3550.
60 H. G. Zhu, D. Y. Chen, A. Wei, N. J. Li, Q. F. Xu, H. Li, J. H. He and J. M. Lu, *Small*, 2015, **11**, 5222–5229.
61 S. Y. Gao, X. G. Li, L. Y. Li and X. J. Wei, *Nano Energy*, 2017, **33**, 334–342.
62 S. Wang, X. W. Peng, L. X. Zhong, J. W. Tan, S. S. Jing, X. F. Cao, W. Chen, C. F. Liu and R. C. Sun, *J. Mater. Chem. A*, 2015, **3**, 8772–8781.
63 X. J. Gao, X. F. Wang, X. P. Ouyang and C. Wen, *Sci. Rep.*, 2016, **6**, 27207–27214.
64 H. Y. Mi, X. Jing, A. L. Politowicz, E. Chen, H. X. Huang and L.-S. Turng, *Carbon*, 2018, **132**, 199–209.
65 Y. G. Zhang, Y. J. Zhu, Z. C. Xiong, J. Wu and F. Chen, *ACS Appl. Mater. Interfaces*, 2018, **10**, 13019–13027.
66 H. Guan, Z. Y. Cheng and X. Q. Wang, *ACS Nano*, 2018, **12**, 10365–10373.
67 L. R. Shi, K. Chen, R. Du, A. Bachmatiuk, M. H. Rummeli, K. W. Xie, Y. Y. Huang, Y. F. Zhang and Z. F. Liu, *J. Am. Chem. Soc.*, 2016, **138**, 6360–6363.
68 J. W. Lu, D. D. Xu, J. K. Wei, S. Yan and R. Xiao, *ACS Appl. Mater. Interfaces*, 2017, **9**, 25533–25541.
69 J. F. Chen, X. C. Shen, Y. B. Pan, C. Liu, S. Y. Hwang, Q. Xu and Z. M. Peng, *J. Mater. Chem. A*, 2018, **6**, 3996–4002.
70 H. C. Bi, Z. Y. Yin, X. H. Cao, X. Xie, C. L. Tan, X. Huang, B. Chen, F. T. Chen, Q. L. Yang, X. Y. Bu, X. H. Lu, L. T. Sun and H. Zhang, *Adv. Mater.*, 2013, **25**, 5916–5921.
71 L. X. Li, T. Hu, H. X. Sun, J. P. Zhang and A. Q. Wang, *ACS Appl. Mater. Interfaces*, 2017, **9**, 18001–18007.
72 L. Li, B. Li, H. Sun and J. Zhang, *J. Mater. Chem. A*, 2017, **5**, 14858–14864.
73 X. Ge, W. Qin, H. Zhang, G. Wang, Y. Zhang and C. Yu, *Nanoscale*, 2019, **11**, 12161–12168.
74 M. Toyodaa and M. Inagakib, *Carbon*, 2000, **38**, 199–210.
75 P. Song, J. Di, L. X. Kang, M. Z. Xu, B. J. Tang, J. Xiong, J. W. Cui, Q. S. Zeng, J. D. Zhou, Y. M. He, Q. D. Fu, J. Peng, S. S. Guo, B. Lin, J. Y. Zhang, P. Meng and Z. Liu, *Nano-indentation Mater. Sci.*, 2019, **1**, 310–317.
76 D. Sylvain, S. Eduardo, N. Ravi K and T. Antoni P, *Science*, 2006, **311**, 515–518.
77 P. Song, H. L. Qin, H. L. Gao, H. P. Cong and S. H. Yu, *Nat. Commun.*, 2018, **9**, 2786–2794.
78 S. Deville, E. Maire, G. Bernard-Granger, A. Lasalle, A. Bogner, C. Gauthier, J. Leloup and C. Guizard, *Nat. Mater.*, 2009, **8**, 966–972.
79 M. Li, C. Bian, G. Yang and X. Qiang, *Chem. Eng. J.*, 2019, **368**, 350–358.
80 Z. Lei, P. Zheng, L. Niu, Y. Yang, J. Shen, W. Zhang and C. Wang, *Appl. Surf. Sci.*, 2019, **489**, 922–929.
81 S. Zhou, G. Hao, X. Zhou, W. Jiang, T. H. Wang, N. Zhang and L. H. Yu, *Chem. Eng. J.*, 2016, **302**, 155–162.

